Effect of Crack Length on Fracture Behavior of Particleboard

Yan Wang,[a,*] and Arif Caglar Konukcu [b]

The effect of crack length on the fracture behavior of particleboard was investigated using the single-edge-notched bending (SENB) test method under mode I loading. The initial slope (k_{init}), critical stress intensity factor (K_{IC}), specific fracture energy (G_f), and brittleness number were calculated for five different crack length/specimen width (*a/W*) ratios varying from 0.1 to 0.9 at intervals of 0.2. The results show that the fracture properties were significantly higher for specimens with an *a/W* ratio of 0.1 than for the others. However, for the critical stress intensity factor and specific fracture energy, there were no significant differences among the *a/W* ratios of 0.3, 0.5, and 0.7 where the crack tip was placed in the core layer of the particleboard. In general, as the *a/W* ratio decreased, the stiffness of the material increased, and the specimens with an *a/W* ratio of 0.1 showed brittle behavior. However, there was no statistically significant difference between *a/W* ratios of 0.5 and 0.7.

DOI: 10.15376/biores.18.1.175-186

Keywords: Particleboard; Fracture; Crack size; Fracture toughness; Specific fracture energy

*Contact information: a: College of Engineering and Design, Hunan Normal University, Changsha 410081, China; b: Department of Forest Industrial Engineering, Faculty of Forestry, Izmir Katip Celebi University, Izmir 35620, Turkey; *Corresponding author: wangyan042018@163.com*

INTRODUCTION

Particleboard (PB) is a well-known wood-based composite made of wood particles bonded together with various adhesives. It has broad uses in furniture industries. The physical and mechanical properties of PB are mainly determined by the components, such as wood geometry of particle, adhesive type, and compression technology (pressure and temperature). A typical PB consists of three layers including two face layers made of fine wood particles and one core layer that is made of coarser particles. The PB usually has good performance on dimensional stability (Rowell *et al.* 1986), fastener bearing capacity (Hu and Zhang 2020, 2021), and is inexpensive compared to natural solid wood.

In general, there are many studies on the fracture mechanical properties of wood and wood-based composite materials (Beer *et al*. 2008; Rathke *et al.* 2012a; Veigel *et al*. 2012; Marsavina *et al.* 2018; Scorza *et al.* 2019; Hu *et al*. 2021; Hu and Zhang 2022). Although PB is one of the most important wood-based composite materials, few investigations on its fracture behavior have been done. The PB is a highly heterogeneous material at the millimeter scale due to the size of the particles. According to Sinn *et al.* (2008), the difficulty in describing the materials grows as their structure becomes more heterogeneous. Although the mechanical properties of three-layer PB such as strength and elasticity have received much attention in the literature, little is known about the fracture properties of PB. Therefore, it is necessary to have a good understanding of the fracture properties of PB, which is widely used for construction and furniture manufacturing. The

fracture behavior of the wood-based composite can be evaluated using a variety of specimen configurations subjected to tensile, shear, or bending loads, *i.e*., single-edge-notched bending (SENB) (Yoshihara 2010a; Yoshihara and Mizuno 2014; Marsavina *et al.* 2018; Huang and Wang 2022), single-edge-notched tension (SENT) (Yoshihara 2010b), compact tension (CT) (Yoshihara and Usuki 2011), and double cantilever beam (DCB) (Rathke *et al.* 2012a; Veigel *et al*. 2012).

Concerning the fracture mechanical properties of PB, Beer *et al*. (2005) determined the fracture energy using microtome cutting tests and compared their findings with those obtained from wedge-splitting tests. Their results showed that materials can be physically characterized and compared using the specific fracture energy determined by nonlinear elastic fracture mechanics. The effect of size on the fracture toughness was investigated by Scorza *et al.* (2019) using different geometric sizes of notched PB beams tested under three-point bending. The fracture properties of MDF and PB were also investigated under pure modes I and II and also under the mixed mode loading conditions (Torabi *et al.* 2021). Yoshihara and Mizuno (2014) investigated the effects of crack length on the mode I critical stress intensity factor of medium-density fiberboard (MDF) using the SENB test. The results show that the critical stress intensity factor can be obtained effectively under the crack length/specimen width (*a/W*) ratio ranging from 0.5 to 0.7. Yoshihara (2010b) studied the effect of loading conditions on the measurement of mode I critical stress intensity factor for MDF using the SENT test. The findings of the SENT test were compared to those obtained from the DCB test. The results showed that the critical stress intensity factor values obtained using the SENT and DCB tests were not significantly different between the *a/W* ratios of 0.5 and 0.7. In contrast, the difference is significant at the *a/W* ratios of 0.3 and 0.4, where material nonlinearity occurs before the crack propagation. Rathke *et al.* (2012a) examined the impact of the raw material (spruce, recovered particles, willow, poplar, and locust) on the fracture mechanical properties of PB using the DCB test. The results of specific fracture energy and stress intensity factor of PB show significant differences between raw materials, as well as adhesive composition. Sinn *et al.* (2008) studied the fracture behavior of particleboard containing different amounts of recycling wood with three kinds of melamine coatings. According to the results, the fracture energy in the core layer significantly decreased as the amount of recycling wood particles increased. Higher critical stress intensity factor values also confirmed that the face layer of PB is stronger than the core layer due to higher density. Veigel *et al*. (2012) also investigated the mode I fracture behavior of PB from different adhesives reinforced with cellulose nanofibers using the DCB test method. The results show that the addition of cellulose nanofibers to the adhesive significantly increased the adhesive's bond toughness, resulting in an increase in the fracture energy and fracture toughness of PB. Marsavina *et al.* (2018) studied the fracture toughness of a commercial PB by performing the SENB test and a compact shear test (CS) for Mode I and Mode II, respectively. They also used digital image correlation (DIC) to measure the displacement field near the crack during the fracture test. From their study, the fracture properties, *i.e.*, the relative displacement factor of the crack, the stress intensity factor, and the fracture energy, could be estimated without knowledge of the material properties.

Most previous studies on the fracture mechanical properties evaluated the PB on the panel surface, where cracks propagated along the surface layer. However, in this study, the fracture properties (critical stress intensity factor, initial slope, and specific fracture energy) of PB with a crack out-of-plane (growing throughout the panel thickness) were investigated to evaluate the effects of crack length/specimen width (*a/W*) ratios varied at

five different levels on the fracture mechanical properties of PB. As a result, the effects of density and layer differences along the thickness on the fracture behavior of the particleboard were considered.

EXPERIMENTAL

Materials

The PB was provided by Roseburg Particleboard Company (Taylorsville, MS, USA), with a thickness of 21 mm. The average density was 690.4 kg/m^3 with a coefficient of variance (COV) of 1.2%, tested according to the ASTM D2395-17 (2022) standard. The PB was conditioned at a temperature of 20 °C and a relative humidity of 42% for two weeks prior to specimen preparation. The conditioning process was carried out according to the ASTM D4933-16 (2021) standard.

Specimen Preparation

All SENB test specimens were prepared with the initial crack length, *a*, in the crack opening perpendicular to the board surface. Table 1 lists five different crack sizes and crack length/specimen width (*a/W*) ratios used in the study. The number of specimens was 15 for each *a/W* ratio. A 1-mm-thick crack (Figs. 1 and 2) was first cut out with a band saw to create the initial crack. A razor blade was then used to create a 1-mm-long, extended, sharp crack tip. The crack length varied from 2.1 to 18.9 mm at five different levels. Thus, the *a/W* ratios ranged from 0.1 to 0.9 at intervals of 0.2. The thickness was constant at 15 mm for all test specimens.

Table 1. Crack Sizes and *a/W* Ratios Used in the Study

Crack Location	Crack Length "*a*" (mm)	Width "*W*" (mm)	*a/W* Ratio
Face Layer (0 to 4.1 mm)	2.1	21	0.1
Core Layer (4.1 to 16.9 mm)	6.3	21	0.3
	10.5	21	0.5
	14.7	21	0.7
Face Layer (16.9 to 21 mm)	18.9	21	0.9

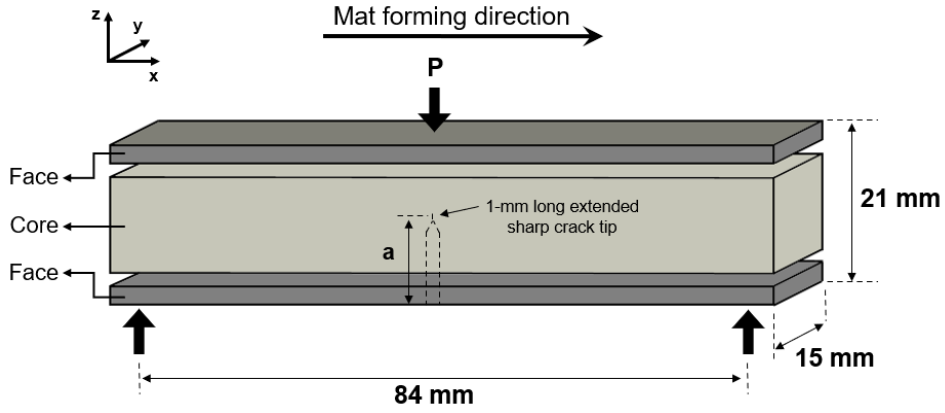

Fig. 1. The general configuration of the mode I SENB test block with PB layers; x, mat-forming direction; y, perpendicular to the mat forming direction; z, perpendicular to the board surface

All testing samples were placed in the conditioned humidity chamber with its condition controlled at a temperature of 20 °C and relative humidity of 42% for two weeks prior to fracture properties testing (ASTM D4933-16).

Testing Methods

Density profile

The density profiles of PB samples in end grain were measured using a QMS density profiler (Model QDP-01X, Quintek Measurement Systems, Inc., Knoxville, TN, USA) testing machine with the dimensions of sample 51 mm× 51mm × 21 mm.

Fracture properties

A standardized test method for determining the fracture toughness of wood-based composites has not been established yet. Therefore, ASTM E399-22 (2022) standard for metallic materials was used as a reference for the test. Figure 2 shows the setup for performing a SENB test on a fracture toughness test block following the ASTM E399-22 (2022) standard. Mode I SENB tests were performed on an INSTRON 5566 (Instron, Norwood, MA, USA) universal testing machine. The load *P* was applied at a crosshead with a speed of 0.5 mm/min (Yoshihara and Mizuno 2014). The load-deformation curves of all tested specimens were loaded until a noticeably propagated crack appeared and were then recorded. The critical stress intensity factor (K_{IC}), initial slope (k_{init}), and specific fracture energy (G_f) were determined from the load-deformation curves. The critical stress intensity factor was calculated using the following formula (ASTM E399-22),

$$K_{\mathrm{IC}} = \frac{P_{\mathrm{Q}} \times L}{B \times W^{3/2}} \times f\left(\frac{a}{W}\right) \quad (1)$$

where

$$f\left(\frac{a}{W}\right) = 3 \times \sqrt{\frac{a}{W}} \times \frac{1.99 - \left(\frac{a}{W}\right) \times \left(1 - \frac{a}{W}\right)\left[2.15 - 3.93 \times \frac{a}{W} + 2.7 \times \left(\frac{a}{W}\right)^2\right]}{2 \times \left(1 + 2 \times \frac{a}{W}\right) \times \left(1 - \frac{a}{W}\right)^{3/2}} \quad (2)$$

where P_Q is the critical force initiating crack propagation (*N*), *L* is the span length (m), *B* is the thickness of a SENB test specimen (m), *W* is the width of a SENB test specimen (m), and *a* is the initial crack length (m) (Figs. 1 and 2).

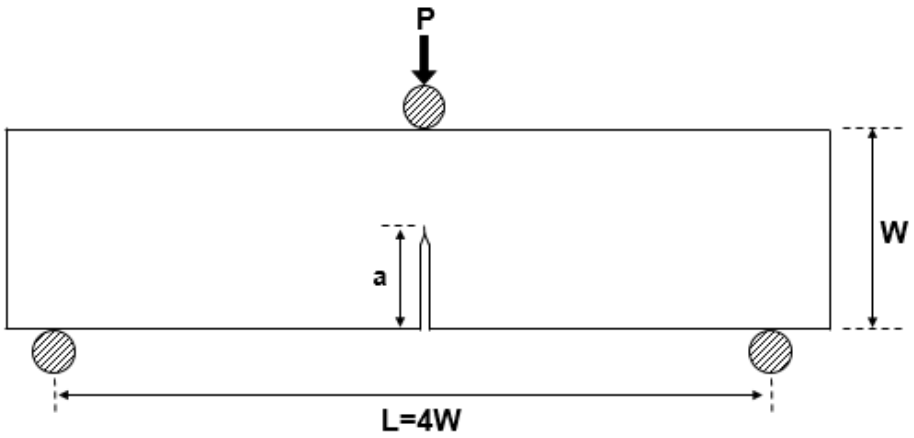

Fig. 2. The Mode I SENB test setup of the study

The critical force initiating crack propagation, P_Q, in Eq. 1 was determined by drawing a tangential line to the initial linear portion of the *P*-δ curve of a tested SENB block (Fig. 3), offsetting this line by a 5% reduction in its slope, and locating the intersection of this offsetting line with the load-deformation curve (*P*-δ) in the failure region (ASTM E399-22). If the maximum force was found earlier than the intersection, then it was defined as the critical force.

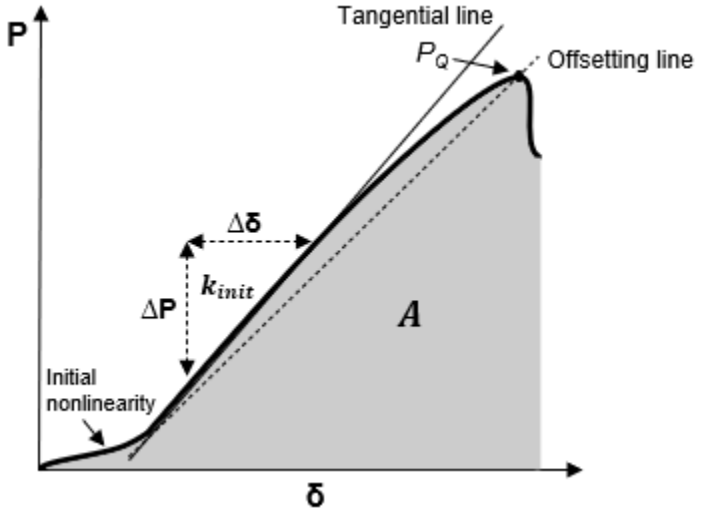

Fig. 3. Graphical illustration showing how a force initiating crack propagation, P_Q, was derived and how the initial slope, k_{init}, and the integrated area, *A*, were defined based on the load-deformation curve

The initial slope of the load-deformation curves in the linear elastic region was determined to characterize the stiffness of the material using the following formula (Majano-Majano *et al*. 2012),

$$k_{init} = \frac{\Delta P}{\Delta \delta} \quad (3)$$

where ΔP is the difference between the upper and lower limit of load within the linear elastic region (*N*), and $\Delta\delta$ is the deflection difference corresponding to ΔP (mm).

The specific fracture energy was calculated from the integrated area under the load-deformation curves (Fig. 3) divided by the area of the fracture surface using the following formula (Majano-Majano *et al*. 2012; Rathke *et al*. 2012b),

$$G_{\mathrm{f}} = \frac{1}{(W-a)*B} \int_0^{\delta_{\max}} P(\delta)\, d\delta \quad (4)$$

where *P* is the applied load (*N*), δ is the deflection at the loading point, *W* is the width of the test specimen (m), *a* is the initial crack length (m), and *B* is the thickness of the test specimen (m).

The brittleness number was calculated to characterize the behavior of each SENB specimen tested using the following formula (Reiterer *et al.* 2002),

$$B = \frac{P_{\max}^2}{L \times k_{\mathrm{init}} \times G_{\mathrm{f}}} \quad (5)$$

where P_{max} is the maximum force (N), and L is the ligament length (m). According to this parameter, lower values indicate ductile behavior of the tested specimen whereas higher values indicate brittle behavior.

Statistical Analysis

One-way analysis of variance (ANOVA) at 95% level of confidence was performed to determine whether there were significant differences among the five *a/W* ratios tested in this study. If the difference among the groups was significant, a comparison was made with Tukey's honestly significant difference test. The SAS 9.4 (SAS Inc., Cary, NC, USA) software was used in statistical analysis.

RESULTS AND DISCUSSION

Density Profile

The density profile of PB at the end grain is shown in Fig. 4, indicating that the density of the face layer was much higher than that of the core layer. Table 2 compares the average densities of the face layer, the core layer, and the entire PB.

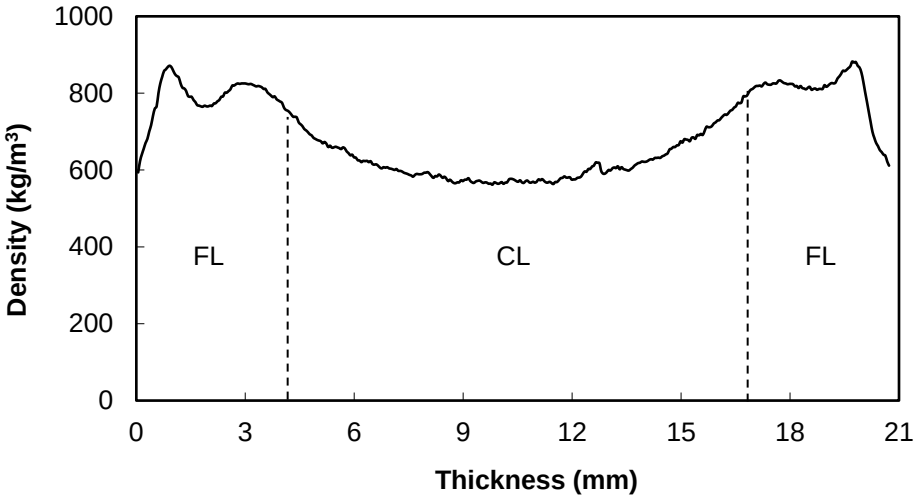

Fig. 4. Typical density profile of tested PB; FL, face layer; CL, core layer

Table 2. Mean Values of Density of Face and Core Layers and Entire Board

	Face Layer	Core Layer	Entire Board
Density (kg/m^3)	792.9 (1.5)	587.9 (1.5)	690.4 (1.2)

Values in parentheses are coefficient of variation in percentage

Fracture Properties

Figure 5 shows typical load-deformation curves for specimens obtained by the SENB test with different *a/W* ratios. The curves clearly show the effects of the *a/W* ratio on the fracture properties of PB. In general, the specimen with an *a/W* ratio of 0.1 had a higher failure load than the others. At an *a/W* ratio of 0.1, the load increased linearly until it reached its maximum, at which point the fracture occurred immediately.

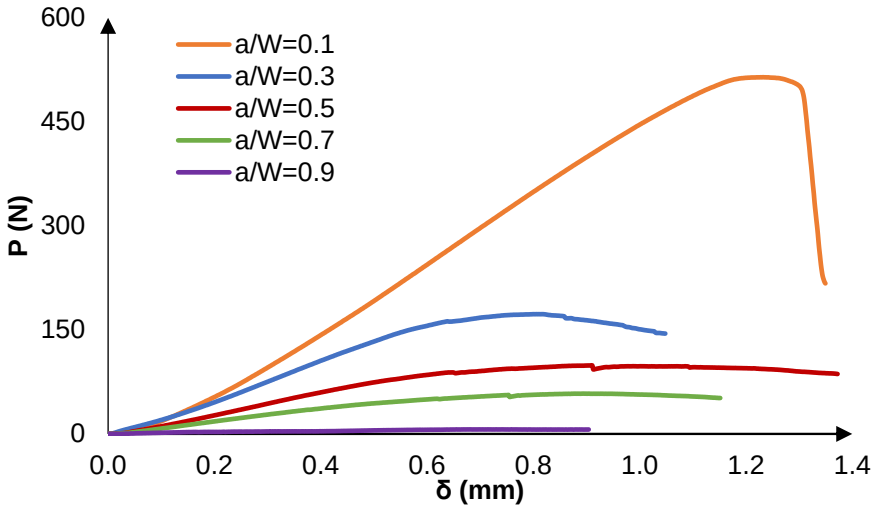

Fig. 5. Typical load-deformation curves for specimens with different *a/W* ratios obtained by the SENB test

Figure 6 shows the relationships between the *a/W* ratio and the fracture properties of PB obtained by the SENB test. The critical stress intensity factor decreased when the *a/W* ratio was increased to 0.3. Thereafter, it stabilized among the *a/W* ratios of 0.3, 0.5, and 0.7 and finally reached its lowest value at a ratio of 0.9 (Fig. 6a). This trend also occurred for specific fracture energy, indicating that the effects of *a/W* ratio on critical stress intensity factor and specific fracture energy were consistent. However, the initial slope decreased linearly as the *a/W* ratio increased (Fig. 6b).

The mean values of these fracture properties were statistically compared. Table 3 shows the one-way ANOVA results of critical force and critical stress intensity factor for five *a/W* ratios of 0.1, 0.3, 0.5, 0.7, and 0.9. In general, the effect of *a/W* ratio on critical force was significant, and the differences between groups were significantly different. The effect of *a/W* ratio on critical stress intensity factor was also significant. The critical stress intensity factor with *a/W* ratio of 0.1 was significantly higher than the others. However, there were no statistical differences among the values with *a/W* ratio of 0.3, 0.5, and 0.7. The results showed that with an increase in the *a/W* ratio of PB from 0.1 to 0.3, the fracture toughness decreased approximately 43%, while the failure load was reduced approximately 68%. The crack tips of the specimens with *a/W* ratio of 0.3, 0.5, and 0.7 were all located in the core layer of PB. It is well known that the density of the core layer of PB is typically lower than the density of the face layer and that density has a significant effect on the fracture toughness of wood-based composites (Reiterer *et al.* 2002; Matsumoto and Nairn 2009, 2012; Scorza *et al.* 2019). The low core layer density of PB is due to coarser particles causing large crack gaps (Sackey *et al.* 2008). Crack propagation is also caused by these large crack gaps. Therefore, the density of the crack tip location mainly affects the crack resistance of PB (Sinn *et al.* 2008; Scorza *et al.* 2019). The fracture properties of wood-based composites are also influenced by additional effects such as fiber bridging, particle size, layering, and particle orientation (Rathke *et al.* 2012b, 2013). The crack length is another factor. Yoshihara (2010a) mentioned that crack propagation is unstable when the *a/W* ratio is less than 0.3, while it is stable when the ratio is higher than 0.4. In line with the findings of this study, Yoshihara and Mizuno (2014) also confirmed that the *a*/*W* ratio should be in the range of 0.5 and 0.7 when determining the critical stress intensity factor value.

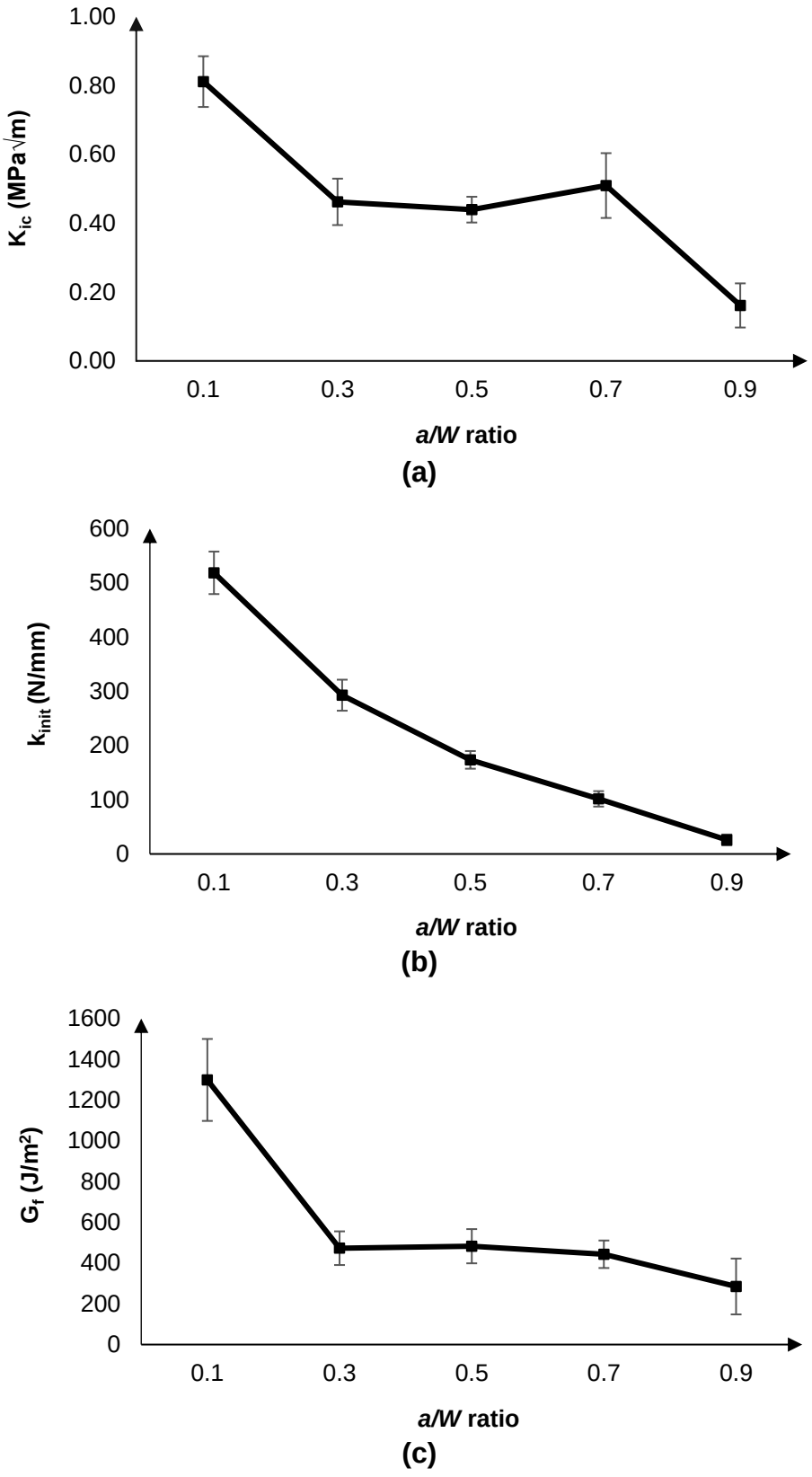

Fig. 6. The effect of *a/W* ratios on fracture properties of the PB: (a) the critical stress intensity factor, K_{IC}, (b) the initial slope, k_{init}, and (c) the specific fracture energy, G_f

Table 3. Comparison Mean Values of the Critical Force and the Critical Stress Intensity Factor for Each *a/W* Ratio in the PB

a/W Ratio	Critical Force (P_Q) (N)	Critical Stress Intensity Factor (K_{IC}) (MPa√m)
0.1	520.65 (47.28) A	0.81 (0.07) A
0.3	165.07 (24.09) B	0.46 (0.07) B
0.5	89.70 (7.64) C	0.44 (0.04) B
0.7	47.32 (8.74) D	0.51 (0.09) B
0.9	2.84 (1.13) E	0.16 (0.06) C

* Values in parentheses are standard deviations; means with the same letter are not significantly different at the 5% significance level

Table 4. Comparison of Mean Values of the Initial Slope, Specific Fracture Energy, and the Brittleness Number for Each *a/W* Ratio in the PB

a/W Ratio	Initial Slope (k_{init}) (N/mm)	Specific Fracture Energy (G_f) (J/m^2)	Brittleness Number (B) (mm)
0.1	518.53 (39.21) A	1298.81 (201.15) A	21.46 (1.26) A
0.3	292.83 (28.60) B	472.98 (82.61) B	13.53 (2.43) B
0.5	173.51 (16.28) C	482.69 (83.97) B	9.69 (1.52) C
0.7	101.66 (14.23) D	443.13 (67.49) B	10.13 (1.64) C
0.9	25.95 (9.95) E	285.03 (136.96) C	6.03 (1.95) D

* Values in parentheses are standard deviations; means with the same letter are not significantly different at the 5% significance level

Table 4 shows the mean comparisons of fracture properties including initial slope, specific fracture energy, and brittleness number for each *a/W* ratio. In general, it can be seen that these fracture properties were significantly affected by the *a/W* ratio. For the initial slope, which indicates the stiffness of the material, there was a significant difference between each *a/W* ratio. For all specimens, the initial slope started with a high value and then decreased linearly with increasing *a/W* ratio. For the specific fracture energy, the value with an *a/W* ratio of 0.1 was significantly higher than the others. However, there were no statistical differences among the values with *a/W* ratio of 0.3, 0.5, and 0.7, which might be due to the fact that the crack tips were located in the core layer of the PB. It was found that the specific fracture energy was higher in the face layers. The results showed that with the increase of *a/W* ratio of PB from 0.1 to 0.3, the specific fracture energy decreased 64%. The higher fracture toughness and specific fracture energy results confirm that the face layers are stronger than the core layers. This means that the crack growing in the PB requires more energy per unit area to separate a specimen into two halves. The results also showed that the ductility of PB increased with increasing *a/W* ratio. The brittleness number at *a/W* ratio of 0.1 was significantly higher than that at 0.3, followed by 0.5, 0.7, and 0.9, but there was no statistical difference between the brittleness numbers at *a/W* ratios of 0.5 and 0.7. Sinn *et al.* (2008) also stated that the face layer of PB behaves more brittle than the entire board. However, the results revealed that, despite being located at the face layer, the ratio of 0.9 was the lowest value for all PB fracture characteristics. Previous studies

explained this situation by stating that when the crack tip gets close to the loading point, the compressive stresses caused by the loading nose hinder self-similar crack propagation (de Moura et al. 2010; Yoshihara and Mizuno 2014).

CONCLUSIONS

The effect of crack length on the fracture mechanical properties of particleboard (PB) was investigated using the single-edged-notched bending (SENB) test method under mode I loading. The main conclusions of this study are as follows:

1. The failure load and stiffness of PB increased while the crack length to specimen width (*a/W*) ratio decreased. The specimens with an *a/W* ratio of 0.1 had significantly higher critical stress intensity factors and specific fracture energy than others. This indicates that the face layer has a greater influence on the fracture stiffness of PB.
2. The specimens with *a/W* ratios of 0.3, 0.5, 0.7, and 0.9 behaved more ductile than the *a/W* ratio of 0.1. There was no significant difference between the *a/W* ratio of 0.3 to 0.7, where the crack tip was in the core layer of the PB, for the critical stress intensity factor and specific fracture energy. The insignificance could be caused by the inherent cracks between the coarser particles in the core layer, which reduce the stiffness.

ACKNOWLEDGMENTS

The authors would like to thank Roseburg Particleboard Company, Taylorsville, Mississippi, for providing particleboard for this study. The authors are also grateful for the support of the Department of Education of Hunan Province, Project No. HNJG-2021-1301.

REFERENCES CITED

ASTM D2395-17 (2022). "Standard test methods for density and specific gravity (relative density) of wood and wood-based materials," ASTM International, West Conshohocken, PA, USA.

ASTM D4933-16 (2021). "Standard guide for moisture conditioning of wood and wood-based materials," ASTM International, West Conshohocken, PA, USA.

ASTM E399-22 (2022). "Standard test method for linear-elastic plane-strain fracture toughness of metallic materials," ASTM International, West Conshohocken, PA, USA.

Beer, P., Gindl, G., and Stanzl-Tscheng, S. (2008). "Wedge splitting experiments on three-layered particleboards and consequences for cutting," *Holz Als Roh-Und Werkstoff* 66(2), 135-141. DOI: 10.1007/s00107-008-0225-9

Beer, P., Sinn, G., Gindl, S., and Stanzl-Tscheng, S. (2005). "Work of fracture and of chips formation during linear cutting of particle-board," *Journal of Materials Processing Technology* 159(2), 224-228. DOI: 10.1016/j.jmatprotec.2004.05.009

De Moura, M. F. S. F., Dourado, N., and Morais, J. J. L. (2010). "Crack equivalent based method applied to wood fracture characterization using the single edge notched three

point bending test," *Engineering Fracture Mechanics* 77(3), 510-520. DOI: 10.1016/j.engfracmech.2009.10.008

Hu, W., and Zhang, J. (2020). "Bolt-bearing yield strength of three-layered cross-laminated timber treated with phenol formaldehyde resin," *Forests* 11(5), article no. 551. DOI: 10.3390/f11050551

Hu, W., and Zhang, J. (2021). "Study on static lateral load–slip behavior of single-shear stapled connections in plywood for upholstered furniture frame construction," *Journal of Wood Science* 61(1), article no. 40. DOI: 10.1186/s10086-021-01975-7

Hu, W., Liu, Y., and Li, S. (2021). "Characterizing mode I fracture behaviors of wood using compact tension in selected system crack propagation," *Forests* 12(10), article no. 1369. DOI: 10.3390/f12101369

Hu, W., and Zhang, J. (2022). "Effect of growth rings on acoustic emission characteristic signals of southern yellow pine wood cracked in mode I," *Construction and Building Materials* 329(1), article ID 12709. DOI: 10.1016/j.conbuildmat.2022.127092

Huang, Y., and Wang, X. (2022). "On the fracture toughness testing for single-edge notched bend specimen of orthotropic materials," *Composite Structures* 281, article no. 114970. DOI: 10.1016/j.compstruct.2021.114970

Majano-Majano, A., Hughes, M., and Fernandez-Cabo, J. L. (2012). "The fracture toughness and properties of thermally modified beech and ash at different moisture contents," *Wood Science and Technology* 46(1-3), 5-21. DOI: 10.1007/s00226-010-0389-4

Marsavina, L., Pop, O., and Linul, E. (2018). "Mixed mode fracture toughness of particleboard," *Procedia Structure Integrity* 9, 47-54. DOI: 10.1016/j.prostr.2018.06.010

Matsumoto, N., and Nairn, J. A. (2009). "The fracture toughness of medium density fiberboard (MDF) including the effects of fiber bridging and crack–plane interference," *Engineering Fracture Mechanics* 76(18), 2748-2757. DOI: 10.1016/j.engfracmech.2009.04.007

Matsumoto, N., and Nairn, J. A. (2012). "Fracture toughness of wood and wood composites during crack propagation," *Wood and Fiber Science* 44(2), 121-133.

Rathke, J., Riegler, M., Weigl, M., Müller, U., and Sinn, G. (2013). "Analyzing process related, in-plane mechanical variation of high density fiber boards (HDF) across the feed direction," *BioResources* 8(3), 3982-3993.

Rathke, J., Sinn, G., Harm, M., Teischinger, A., Weigl, M., and Müller, U. (2012a). "Effects of alternative raw materials and varying resin content on mechanical and fracture mechanical properties of particle board," *BioResources* 7(3), 2970-2985. DOI: 10.15376/biores.7.3.2970-2985

Rathke, J., Sinn, G., Harm, M., Teischinger, A., Weigl, M., and Müller, U. (2012b). "Fracture energy *vs.* internal bond strength–mechanical characterization of wood-based panels," *Wood Material Science & Engineering* 7(4), 176-185. DOI: 10.1080/17480272.2012.699979

Reiterer, A., Sinn, G., and Stanzl-Tschegg, S. E. (2002). "Fracture characteristics of different wood species under mode I loading perpendicular to the grain," *Materials Science and Engineering: A* 332(1-2), 29-36. DOI: 10.1016/S0921-5093(01)01721-X

Rowell, R. M., Sirnonson, R., and Tillrnan, A. M. (1986). "Dimensional stability of particleboard," *Nordic Pulp & Paper Research Journal* 1(2), 11-17. DOI: 10.3183/NPPRJ-1986-01-02-p011-017

Sackey, E. K., Semple, K. E., Oh, S. W., and Smith, G. D. (2008). "Improving core bond strength of particleboard through particle size redistribution," *Wood and Fiber Science* 40(2), 214-224.

Scorza, D., Marsavina, L., Carpinteri, A., Ronchei, C., and Vantadori, A. (2019). "Size-effect independence of particleboard fracture toughness," *Composite Structure* 229(3), article ID 111374. DOI: 10.1016/j.compstruct.2019.111374

Sinn, G., Beer, P., Gindl, M., and Stanzl-Tschegg, S. (2008). "Wedge splitting experiments on three-layered particleboard and consequences for cutting," *Holz Roh Werkst* 66, 135-141. DOI: 10.1007/s00107-008-0225-9

Torabi, E., Ghouli, S., Marșavina, L., and Ayatollahi, M. R. (2021). "Mixed mode fracture behavior of short-particle engineered wood," *Theoretical and Applied Fracture Mechanics* 115, article no. 103054. DOI: 10.1016/j.tafmec.2021.103054

Veigel, S., Rathke, J., Weigl, M., and Gindl-Altmutter, W. (2012). "Particle board and oriented strand board prepared with nanocellulose-reinforced adhesive," *Journal of Nanomaterials* 2012, article ID 158503. DOI: 10.1155/2012/158503

Yoshihara, H. (2010a). "Examination of the mode I critical stress intensity factor of wood obtained by single-edge notched bending test," *Holzforschung* 64(4), 501-509. DOI: 10.1515/hf.2010.083

Yoshihara, H. (2010b). "Influence of loading conditions on the measurement of mode I critical stress intensity factor for wood and medium-density fiberboard by the single-edge-notched tension test," *Holzforschung* 64(6), 735-745. DOI: 10.1515/hf.2010.119

Yoshihara, H., and Usuki, A. (2011). "Mode I critical stress intensity factor of wood and medium-density fibreboard measured by compact tension test," *Holzforschung* 65(5), 729-735. DOI: 10.1515/hf.2011.063

Yoshihara, H., and Mizuno, H. (2014). "Mode I critical stress intensity factor of medium-density fiberboard obtained by single-edge-notched bending test," *Drvna Industrija* 65(2), 99-104. DOI: 10.5552/drind.2014.1326

Article submitted: August 18, 2022; Peer review completed: October 15, 2022; Revised version received: October 27, 2022; Published: November 4, 2022.
DOI: 10.15376/biores.18.1.175-186